JOURNAL OF MATERIALS SCIENCE **34** (1999) 3127–3135

Sol-gel/co-precipitation method for the preparation and characterization of zirconia-tungsten composite powders

S. VIVES
LMIT, Pole universitaire du pays de Montbeliard, 4 place Tarradin, BP 427, 25200 Montbeliard, France

C. GUIZARD, L. COT
LMPM, UMR 5635-CNRS, ENSCM, 8 rue de l'école normale, 34296 Montpellier cedex 5, France

C. OBERLIN
Electricité De France, Département Application de l'Electricité dans l'Industrie, Centre des Renardières, Route de Sens BP1, 77250 Moret sur Loing, France
E-mail: serge.vives@pu-pm.univ-fcomte.fr

Sol-gel and co-precipitation are interesting processes in view to prepare ceramic-metal composite powder. Using metal salts as starting compounds it is possible in a first step to synthetise a mixed precipitate and in a second reduction step, in a H_2/Ar atmosphere, to obtain such a composite powder. Stabilized zirconia-tungsten composite powder have been prepared by this way without mixing and milling steps. Each step of the synthesis has been characterized. Stability of the mixed precipitate suspension and surface area of the dried powder are largely influenced by the tungsten salts content. The temperature of formation of zirconia changes from 510 °C without tungsten precursor up to 695 °C for a 60% tungsten molar ratio composition. Composite zirconia-tungsten powders, in a large range of composition, are obtained at 1100 °C with morphologies depending on humidity and thermal treatment conditions.

1. Introduction

The coprecipitation process is a very convenient method for oxide powders synthesis [1]. For zirconates a number of powder preparations by the coprecipitation method have been reported in the literature using nitrate, chloride and oxichloride salts as starting materials [2–4]. The preparation of Y_2O_3 stabilized ZrO_2 has been described as a three steps process [4] in which yttrium and zirconium salts are hydrolised in basic medium, then transformed in a hydrated gel and a subsequent dried powder at 100–300 °C, and finally crystallized at 400 °C. The coprecipitation method has also been applied to cerium-zirconium double oxide preparation from nitrate salts [5]. In recent years the sol-gel process has been mentioned as a suitable method for the preparation of metal-ceramic materials [6]. These materials exist under different shapes and composite structures as powders, thin films, bulk materials, dense or porous materials with the metal phase below or above the percolation threshold. Furthermore ceramic-metal materials can be used in different applications as electric, mechanic and catalyst [7–10]. Compared to the conventional methods in which metal is infiltrated in a ceramic matrix or mixed and milled with a ceramic powder before sintering, the sol-gel approach allows the preparation by a chemical method of mixed powders in which the metal precursor is present at the molecular level. The preparation of metal-oxide composite such as Cu–Al_2O_3 [6], Ni–Al_2O_3 [11, 12] and Ni–ZrO_2 [13] has been described starting from oxide-oxide biphasic gel or from polymerized monophasic oxide gel containing M–O–M′ chemical bounds. In these powders the metallic phase is formed by powder heating or sintering under reducing atmospheres.

In the present work, we present a preparation method combining the basic concepts of both co-precipitation and sol-gel processes for the synthesis of composite zirconia-tungsten powders. Such powders are of interest in the preparation of cermets exhibiting a mixed electronic-ionic conductivity, leading to a Joule heating effect at low temperature through electric conductivity (tungsten metal contribution) and at high temperature through ionic conductivity (zirconia ceramic contribution).

2. Experimental

2.1. Powder synthesis

Two solutions containing the ceramic and metal precursors are prepared in a first step. The first one was obtained by the dissolution of $ZrOCl_2 \cdot 8H_2O$ (Fluka) and $YCl_3 \cdot 6H_2O$ (Aldrich) in distilled water, the molar ratio

between yttrium salt and zirconium salts has been chosen in order to obtain stabilized zirconia with composition $(ZrO_2)_{0.9}(Y_2O_3)_{0.1}$ and the concentration of zirconium salt has been fixed at 0.5 M. The pH of this solution is in the acid range ($1 < pH < 2$). The second one was prepared by the dissolution of $Na_2WO_4{\cdot}xH_2O$ (Alfa) in distilled water with 0.5 M concentration. The pH of the solution was in the range 9–12. The next step consists in a mixed precipitate formation by slowly adding the tungsten salt solution to the zirconium/yttrium salts solution. The pH was then adjusted to neutrality ($pH \sim 7$) by the introduction of an ammonia solution or a hydrochloric acid solution depending on the final pH of the reaction medium. In a third step the precipitate is washed by centrifugation using distilled water in order to remove Cl^- and Na^+ ions. Indeed sodium ions could alloy with tungsten oxide to form tungsten bronze which generate a liquid phase during the reduction step. In the final step, after drying (110 °C/3 h) the precipitate is fired in a H_2/Ar (10/90) atmosphere up to 1100 °C/5 h. Intermediate firing temperatures (550, 750 and 1000 °C) have been used in order to characterize intermediate structures formed in the powder material during the heat treatment. This reduction treatment produced a ceramic-metal composite powder. The final mixed powder composition is given by the $N_W/(N_W + N_{Zr})$ ratio where N_i is the number of moles of the i constituent knowing that $(N_Y/2)/[(N_Y/2) + N_{Zr}] = 0.1$ for all the composite powders. A scheme of the synthesis is given in Fig. 1.

2.2. Characterization methods

A microelectrophoresis apparatus (Brother Mark II) was used to measure electrophoretic mobility and to determine the IEP (isoelectric point) of the dried (110 °C) particulate precipitate. pH was adjusted to the desired value through the addition of an ammonia or a hydrochloric acid solution.

Density of dried precipitates were measured using a Micromeretics 1305 multivolume helium pycnometer. Samples were outgased at room temperature during one hour. The specific surface area of the samples were measured applying the Brunauer Emnet and Teller (BET) method with a Micromeretics ASAP 2000 apparatus. The samples were outgased at 300 °C for 24 h and the adsorbate gas was nitrogen.

X-ray diffraction patterns were recorded using a Inel CPS 120 diffractometer with CuK_α radiation. The IR spectra, in the absorbance mode, were recorded on a FTIR Nicolet 5ZD spectrometer between 4000 and 400 cm^{-1}.

DTA measurements were performed up to 1200 °C with a Netzch apparatus in a flowing 10/90 H_2–Ar (20 ml min^{-1}) atmosphere. TGA analysis were carried out up to 900 °C in a flowing 10/90 H_2–Ar (20 ml min^{-1}) atmosphere using a SETARAM B85 apparatus. For both DTA and TGA measurements the heating rate was 10 °C min^{-1}.

The morphology of powders fired at different temperatures has been imaged using a Leica Stereoscan 260 Scanning Electron Microscope.

3. Results and discussion

3.1. Dried precipitate

3.1.1. Structure of precipitates

Precipitation of hydrated zirconia by the hydrolisis at room temperature of a zirconium oxychloride solution usually leads to an amorphous compound, and

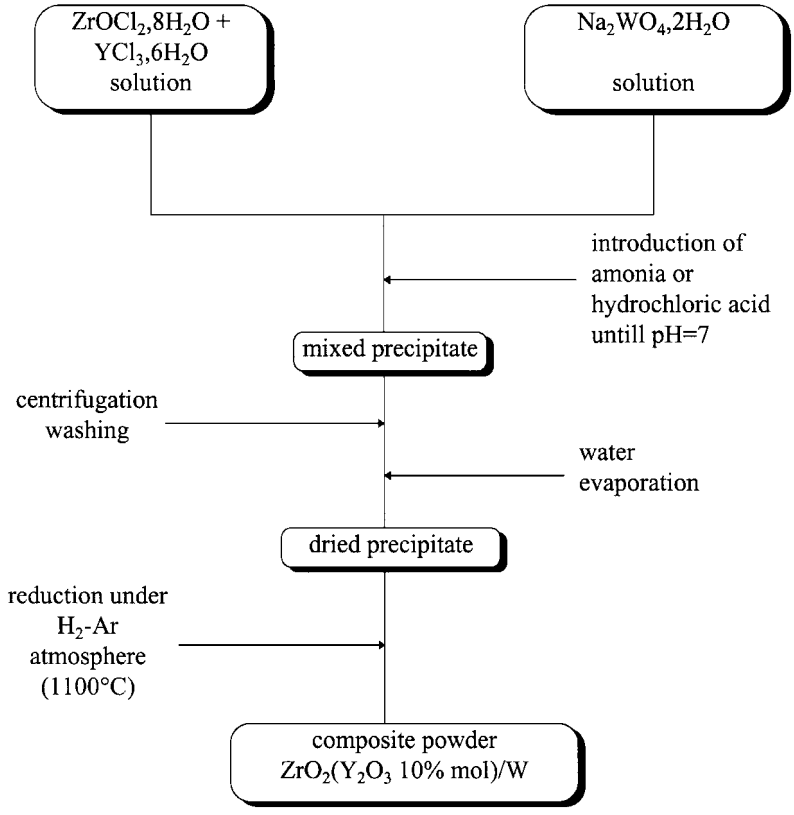

Figure 1 Scheme of the synthesis.

acidification of a sodium tungstate solution leads to a crystallized $WO_3 \cdot xH_2O$ precipitate. In this work the above mentioned method yielded amorphous precipitates even for composition up to $N_W/(N_W + N_{Zr}) = 0.8$, hence it seems that tungsten species do not precipitate under a crystallized particulate compound or that crystallites are too small to be detected by X-ray diffraction.

3.1.2. Powders electrophoretic mobility and IEP determination

During mobility measurements under direct current voltage only one particle population was detected. This means that zirconia and tungsten oxide species are tightly bonded in the precipitate and each particle has the same electrical surface charge probably due to a uniform chemical composition. IEP values of stabilized zirconia and tungsten oxide from the literature [14] are compared in Table I with the prepared powders. Results of electrophoretic measurements and IEP determination are shown in Fig. 2. At pH = 7, which is the final pH during synthesis, an increase of particles mobility under negative voltages as well as a shift of IEP to acidic pH were evidenced with the increase of the $N_W/(N_W + N_{Zr})$ ratio. This result has been attributed to a higher electrical surface charge density due to the presence of negative tungsten oxide species like WO_4^{2-} which are probably adsorbed on the amorphous zirconia surface. Due to a greater repulsive strength between particles an improved suspension stability can be expected for these powders over practically the whole range of pH.

TABLE I Comparison of IEP values from literature with those obtained in this work

Composition	IEP (literature)	IEP (this work)
$ZrO_2(Y_2O_3)$	6.7	6.9
$N_W/(N_W + N_{Zr}) = 0.3$	—	5.1
$N_W/(N_W + N_{Zr}) = 0.5$	—	3.2
$N_W/(N_W + N_{Zr}) = 0.7$	—	1.3
WO_3	0.4	—

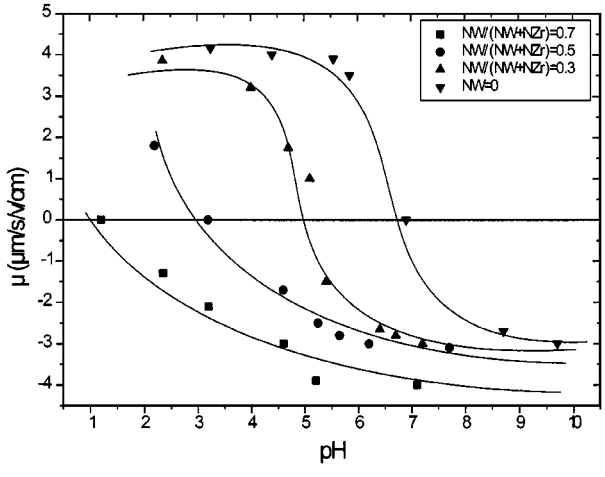

Figure 2 Electrophoretic mobility measurements for various precipitate composition.

TABLE II Measured and calculated densities (additive law) for various precipitates

	Density (g/cm^3)		Additive law density (g/cm^3)	
$N_W/(N_W + N_{Zr})$	25 °C	250 °C	25 °C	250 °C
0 [$ZrO_2(Y_2O_3)$]	4.1	5.2	4.1	5.2
0.3	4.6	5.4	4.9	5.8
0.5	4.9	6.1	5.4	6.3
0.75	5.2	6.5	6	6.8
1 [WO_3]	6.7	7.3	6.7	7.3

TABLE III Vibration bands for ZrO_2 and WO_3

Vibration	WO_3	ZrO_2
ν(OH)	$\sim$3400 cm^{-1}	$\sim$3400 cm^{-1}
δ(OH)	$\sim$1620 cm^{-1}	$\sim$1620 cm^{-1}
ν(M=O)	$\sim$950 cm^{-1}	
ν(O–M–O)	$\sim$680 cm^{-1}	$\sim$450 cm^{-1}

3.1.3. Density of mixed precipitates

Measured and calculated densities of several mixed precipitates are reported in Table II. It can be noted that the density increases with the $N_W/(N_W + N_{Zr})$ ratio. WO_3 has the highest density under its crystallized form. Increasing values result from the high molecular weight of tungsten ($MW = 183.85$ g/mol) present in the structure. The introduction of those heavy species in the structure is then not compensated for a large volume expansion confirming the very tight bonds between zirconia surface and tungsten species. Indeed if $ZrO_2(Y_2O_3)$ and WO_3 were separated, with very small WO_3 cristallite size, additive law of density will give highest values (Table II). After drying at 250 °C the water trapped in the structure evaporates and precipitates become more dense.

3.1.4. Infrared study

Infrared absorption bands characteristic of ZrO_2 and WO_3 compounds are listed in Table III [15–17]. These two oxides behave differently in the 400–1000 cm^{-1} region. A ν(O–Zr–O) absorption band at 465 cm^{-1} is noted for ZrO_2 whereas with WO_3 two absorption bands, ν(O–W–O) and ν(W=O) exist at 680 and 950 cm^{-1}. We can note that zirconia is not characterized by a M=O double bound. The W=O double bond for WO_3 is described [16–17] as a short bond due to the hydratation of the octahedral structure (octahedral sheets separated by H_2O layers). Infrared absorption spectra of mixed precipitates were interpreted in comparison with spectra of amorphous zirconia obtained from zirconium oxychloride and yttrium chloride solution and with spectra of $WO_3 \cdot xH_2O$ obtained by acidification of sodium tungstate solution (Fig. 3). The presence of the ν(O–Zr–O) absorption band near 460 cm^{-1} and the ν(O–W–O) one near 660 cm^{-1} is revealed in every spectra. The band at 1410 cm^{-1} has been interpreted as an absorption due to the presence of ammonium ions on the particles surface arising from the synthesis of zirconia and mixed powders. This

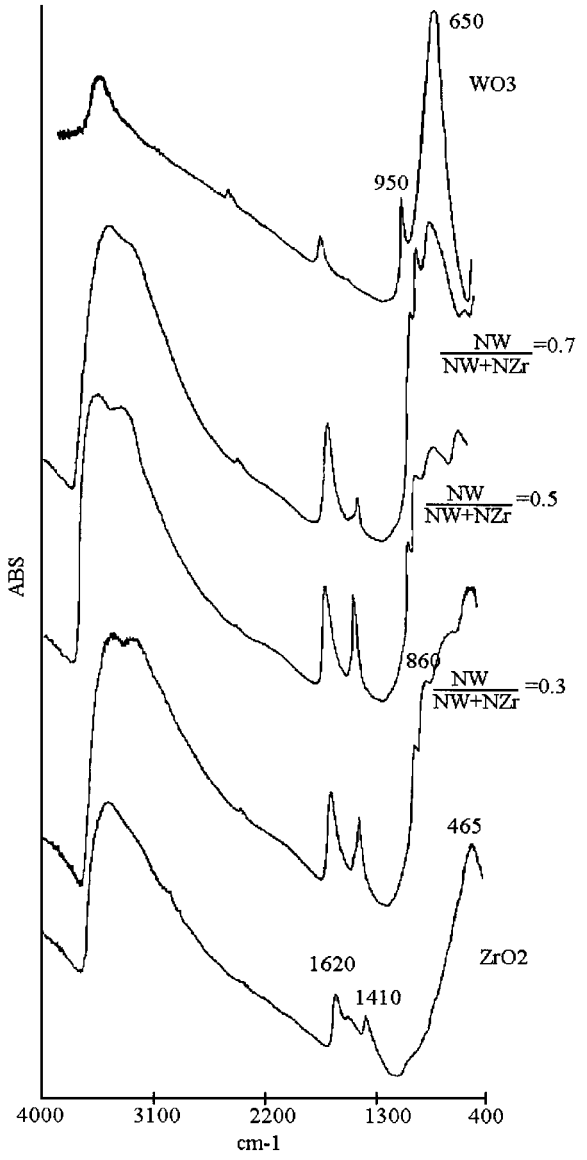

Figure 3 Infrared absorption spectra for various precipitate composition.

absorption band is not present on $WO_3 \cdot xH_2O$ spectra, indeed this compound has been synthesized in acidic medium. In the high wave number range we observe a double peak for mixed precipitates spectra. The first one at 3400 cm^{-1}, present in every spectra, has been attributed to the ν(OH) vibration, the second one at 3250 cm^{-1} only exists for mixed precipitate spectra. According to the literature [16], this band is described as a second harmonic of the δ(OH) (1620 cm^{-1}) vibration but that does not explain why in our case it is only present on the mixed precipitates spectra. Consistently the intensity of the ν(O–W–O) band (640–680 cm^{-1}) increased and the intensity of ν(O–Zr–O) (450–480 cm^{-1}) decreased when the $N_W/(N_W + N_{Zr})$ ratio was increased. The ν(W=O) band appeared for the composition $N_W/(N_W + N_{Zr}) = 0.3$ and its intensity was not changed when the $N_W/(N_W + N_{Zr})$ ratio was increased. The presence of this band in mixed precipitates spectra has been assumed to be an evidence of an octahedral structure for tungsten oxide species close to the $WO_3 \cdot xH_2O$ one, but not organized in a regular lattice. The vibration band at 860 cm^{-1}, only present

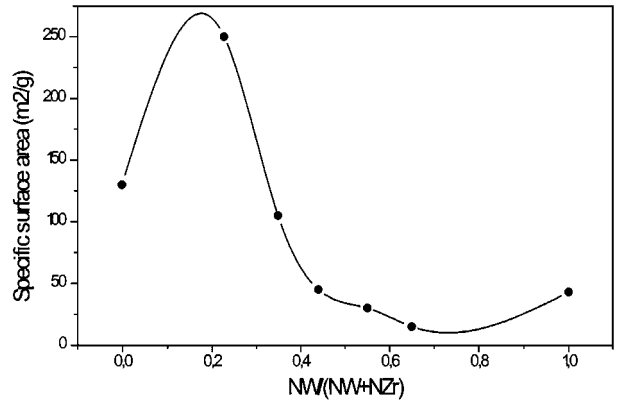

Figure 4 Specific surface area as a function of precipitate composition.

in mixed precipitate spectra, could be due to Zr–O–W bond vibration indicating the existence of a chemical bond between tungsten species and zirconia.

3.1.5. Specific surface area determination

The variation of specific surface area measurements versus precipitate composition is shown in Fig. 4. A maximum was attained for a $N_W/(N_W + N_{Zr}) = 0.2$ composition, afterwards the surface area decreased to a minimum for a $N_W/(N_W + N_{Zr}) = 0.7$ composition. Such a behaviour has been described for a ZrO_2-SiO_2 system [18], obtained by mixing in aqueous solution zirconium nitrate and ethyl silicate and hydrolysing the resulting solution by ammonia. Authors found the highest surface area for a composition of 50% mole of SiO_2. Our results have been interpreted as a competition between two effects. The first one is a dispersion effect due to the adsorption of negative tungsten species on the zirconia surface which has been evidenced by electrophoresis measurements. The second is a particle coarsening which occurs when the $N_W/(N_W + N_{Zr})$ ratio is increased beyond 0.2. If the sole zirconia-yttria precipitate is considered, although the initial grain size can be very small, the pH value ($\sim$7), which is near the IEP value, would normally lead to the formation of hard aggregates. The addition of tungsten precursor salt creates a strong electrostatic effect which avoid the fine grains aggregation thus yielding a larger specific surface area evidenced by the nitrogen adsorption measurements. The efficiency of this dispersive effect due to the adsorption of tungsten is limited to the 0–0.2 composition range. Above 0.2 particle coarsening becomes the more important effect because of an excess of tungsten. The precipitate is still well dispersed but particles get bigger with a decrease in surface area values. Between 0.7 and 1 the slight increase of specific surface area can be explained by the structure of the particles which gets closer to the WO_3 particle crystalline structure.

3.1.6. Evidence of a zirconium-yttrium-tungsten mixed oxide formation

Zirconium and yttrium oxides are known to coprecipitate in the pH range 5–14, on the other hand tungsten salts as sodium tungstate leads to tungsten oxide

TABLE IV X-ray diffraction identification of precipitate for different thermal treatments

Composition	Thermal treatment (H_2/Ar-10/90)	Detected phases
$WO_3 \cdot xH_2O$	550 °C/h	$WO_{2.9}$, WO_3(hex), WO_2
$WO_3 \cdot xH_2O$	750 °C/h	WO_2, $WO_{2.72}$
$WO_3 \cdot xH_2O$	1100 °C/h	W
$N_W/(N_W + N_{Zr}) = 0.6$	600 °C/h	$WO_{2.9}$, WO_3(hex), WO_2
$N_W/(N_W + N_{Zr}) = 0.6$	750 °C/h	ZrO_2(t), WO_2, W
$N_W/(N_W + N_{Zr}) = 0.6$	1000 °C/h	ZrO_2(m), ZrO_2(c), Y_2O_3, WO_2, W
$N_W/(N_W + N_{Zr}) = 0.6$	1100 °C/5 h	ZrO_2(c), W

precipitates only in very acidic solutions (pH < 4). Thus, these two different pH ranges were not in favor of the formation of a coprecipitate with those three oxides. Nevertheless our results show that the resulting amorphous powders contains the three elements, two alternative or concomitant phenomena could explain the homogeneous precipitate formation:

(i) *Coprecipitation:* Olation and oxolation reactions can take place between tungsten and zirconium hydrolized species for a sufficiently acid pH (3–4) in the very first time of the introduction of the tungstate solution in the acidic zirconium-yttrium salt solution.

$$\text{W–OH} + \text{HO–Zr} \rightarrow \text{W–O–Zr} + \text{H}_2\text{O}$$
$$\text{W–OH} + \text{Zr–OH}_2 \rightarrow \text{W–(OH)–Zr} + \text{H}_2\text{O}$$

By this way the tungsten would be trapped inside the structure.

(ii) *Chemical adsorption:* After the addition of the tungsten salt solution, the high pH of this solution allows, in a first step, the fast formation of hydrated zirconia particles. The second step would be the chemical adsorption of the tungsten species on the zirconia particles surface.

$$\text{Zr–OH} + \text{H}_3\text{O}^+ + \text{WO}_4^{2-} \rightarrow \text{Zr–O–W(=O)(=O)–O(−)} + 2\text{H}_2\text{O}$$

This mechanism has been reported for the chemical adsorption of WO_4^{2-} species on alumina particles [19].

Based on the results obtained in this work, coprecipitation and chemical adsorption phenomena could be assumed to occur simultaneously. Hanic *et al.* [20] claim that after firing W^{6+} ions are in interstitial or substitution positions in a fluorite zirconia structure in the case of a WO_3 weight ratio up to 0.1% confirming that tungsten species can be trapped in a zirconia matrix. Hino and Arata [21] have synthesized superacid solids by a simple impregnation of a metatungstate solution on an amorphous zirconia precipitate followed by a calcination step, thus confirming the adsorption way.

Regarding compounds prepared in this work, chemical adsorption is probably the major mechanism. Indeed, ν(O–Zr–O) and ν(O–W–O) vibrations have been evidenced by IRTF spectroscopy for all the compositions under investigation in favor of the presence of unbounded zirconium and tungsten atoms. Furthermore the ν(W=O) vibration always appeared even for a low tungsten precursor content; this vibration would not have been present for an intimately mixed coprecipitate.

3.2. Formation of zirconia-tungsten composite powders under a reduction heat treatment

In view of a better understanding of tungsten oxide reduction under heat treatment in mixed precipitates, a $WO_3 \cdot xH_2O$ precipitate was studied as a reference material under the same conditions (H_2/Ar-10/90 atmosphere). TGA (Fig. 5) and X-ray analysis (Table IV) show that heat treatment with four different temperature ranges would describe the behaviour of the reference powder.

The evaporation of water is observed in the first range (100–400 °C), indeed this mass loss is the sole one observed when TGA is carried out under air atmosphere. Between 400 and 670 °C the mass loss calculation leads to a $WO_{2.72}$ composition whereas the X-ray diffraction pattern of a powder fired at 550 °C reveals the presence of $WO_{2.9}$, hexagonal WO_3 and WO_2 compounds. $WO_{2.9}$ is known to be the first product formed during the WO_3 reduction by pure hydrogen [22]. Furthermore the formation of $WO_{2.72}$ needle shape compound is humidity dependent and the transformation $WO_{2.72} \rightarrow WO_2$ occurs without shape change [23]. In this temperature range water molecules are generated by the reduction reaction itself enhancing

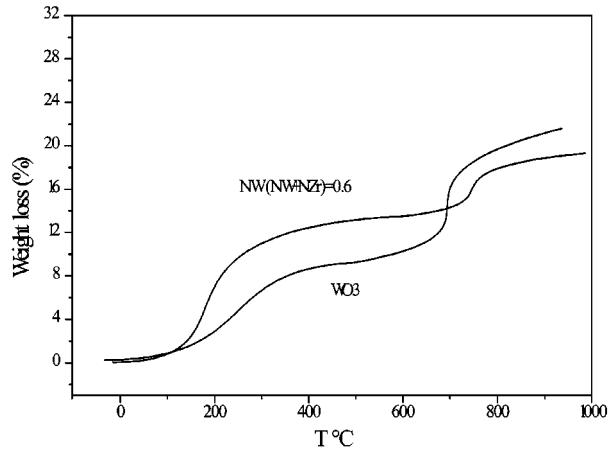

Figure 5 TGA curves for a WO_3 powder and a mixed precipitate.

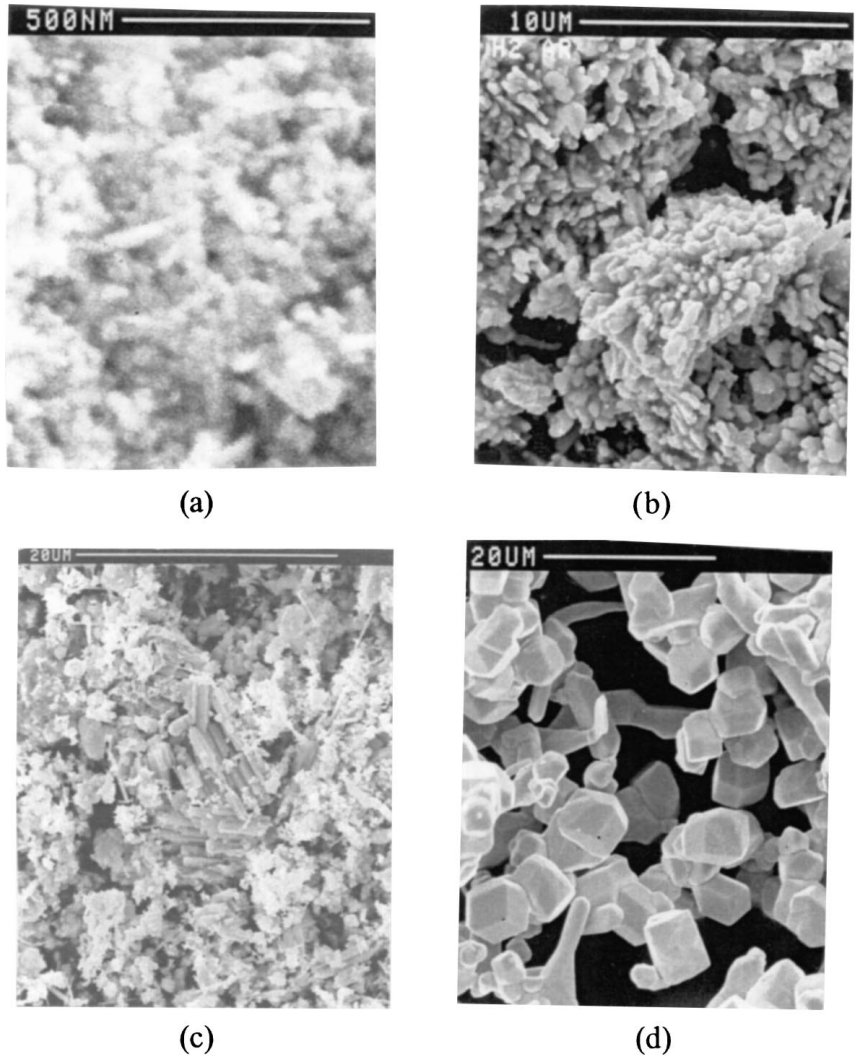

Figure 6 SEM views of a WO_3 powder during the reduction step. (a) dry precipitate, (b) 550 °C/h, (c) 750 °C/h, (d) 1100 °C/h.

the $WO_{2.72}$ formation following the transformation path: $WO_3 \rightarrow WO_{2.9} \rightarrow WO_{2.72}$. On Fig. 6a and b we can observe the effect of the thermal treatment on the powder morphology, the dried precipitate is a nanophase powder whereas at 550 °C the grains are bigger and present an elongated shape.

In the third range (670–880 °C) the mass loss calculation leads to a WO_2 composition and the X-ray diffraction pattern of the powder fired at 750 °C reveals the presence of WO_2 and $WO_{2.72}$ confirmed by the presence of needle shape particles in the powder (Fig. 6c). Thus, in this temperature range, transformation of suboxides to tungsten dioxide occurs.

Above 880 °C the reduction of tungsten dioxide takes place and the entire formation of tungsten metal is achieved at 1100 °C according to X-ray and SEM analysis (Fig. 6d). The following reaction path, including a vapor phase transport process, has been proposed for the reduction of tungsten dioxide [22, 23].

$$WO_2(s) + 2H_2O(g) \rightarrow WO_2(OH)_2(g) + H_2(g)$$

$$WO_2(OH)_2(g) + 3H_2(g) \rightarrow W(s) + 4H_2O$$

This reaction is thermally enhanced but can occur in all the temperature range (500–1100 °C).

For the mixed precipitate of composition $N_W/(N_W + N_{Zr}) = 0.6$ we noted the same four temperature ranges behaviour according to TGA (Fig. 5) and X-ray analysis (Table IV). In the range 100–400 °C the weight loss is due to water evaporation.

In the range 400–700 °C the reduction of WO_3 begins leading to the $WO_{2.72}$ composition. Furthermore D.T.A. measurements (Fig. 7) show an exothermic peak corresponding to the tetragonal ZrO_2 formation. Indeed it is well known that using the sol-gel route tetragonal zirconia is the first crystalline structure which appears during heat treatment [24] and then transforms in the monoclinic structure when the temperature is increased. Under the same conditions, the formation temperature of tetragonal zirconia for the mixed precipitate is 695 °C (Fig. 7b) instead of 510 °C (Fig. 7a) for an amorphous zirconia precipitate obtained from a $ZrOCl_2$ solution. This shift in formation temperatures is probably due to the tungsten oxide compounds bounded with the amorphous zirconia which create a shield like effect inhibiting the phase separation and the formation of tetragonal zirconia. Such a behaviour has been observed for a WO_3/Al_2O_3 system where the transformation $\gamma Al_2O_3 \rightarrow \alpha Al_2O_3$ occurs for a higher temperature [25]. The formation temperature does not vary very much with the precipitate composition; it goes

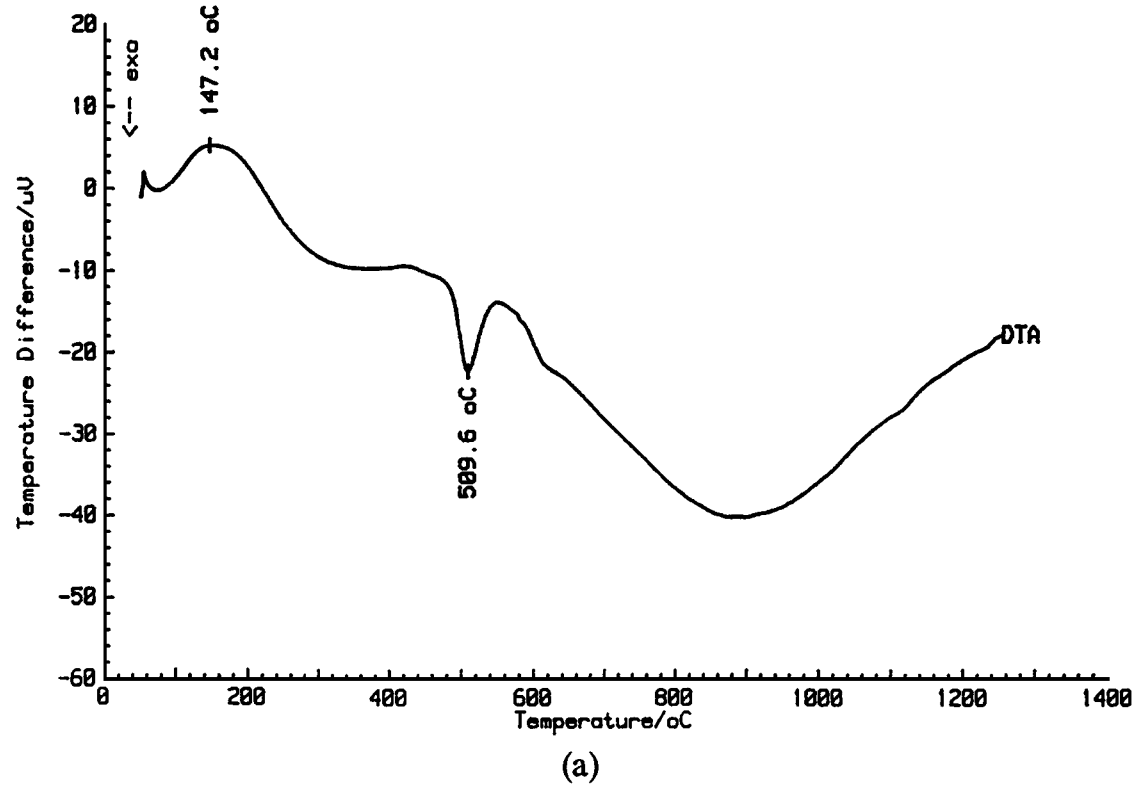

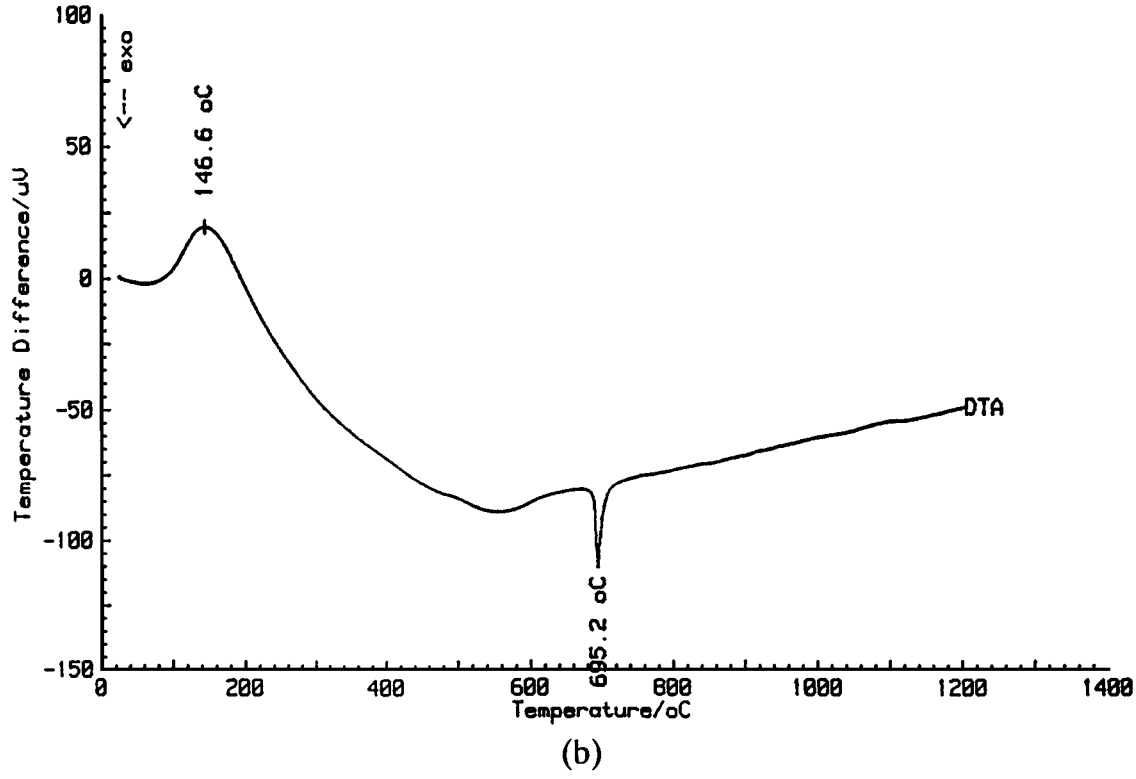

Figure 7 DTA curves for a ZrO_2 precipitate and a mixed precipitate. (a) ZrO_2, (b) $N_W/(N_W + N_{Zr}) = 0.6$.

from 671 °C for $N_W/(N_W + N_{Zr}) = 0.2$ to 695 °C for $N_W/(N_W + N_{Zr}) = 0.6$.

In the 700–900 °C range X-ray diffraction peaks appear corresponding to ZrO_2(t), WO_2, and W. The presence of W in this temperature range could be due to the less humid atmosphere [26, 27] and to the phase separation which generates very small WO_2 grains (large surface area) thus improving the reduction reaction. The humidity is directly linked to the reduction reaction and therefore to the powder amount, indeed for the same Ar/H_2 flow more water molecules will be generated when more tungsten oxide molecules will be present inside the powder. Thus for higher humidity conditions (large amount of powder), $WO_{2.72}$ needle shape compounds were observed by SEM (Fig. 8).

Above 900 °C the complete reduction of tungsten dioxide and the cubic zirconia stabilization occur. Indeed a thermal treatment up to 1100 °C with a dwell

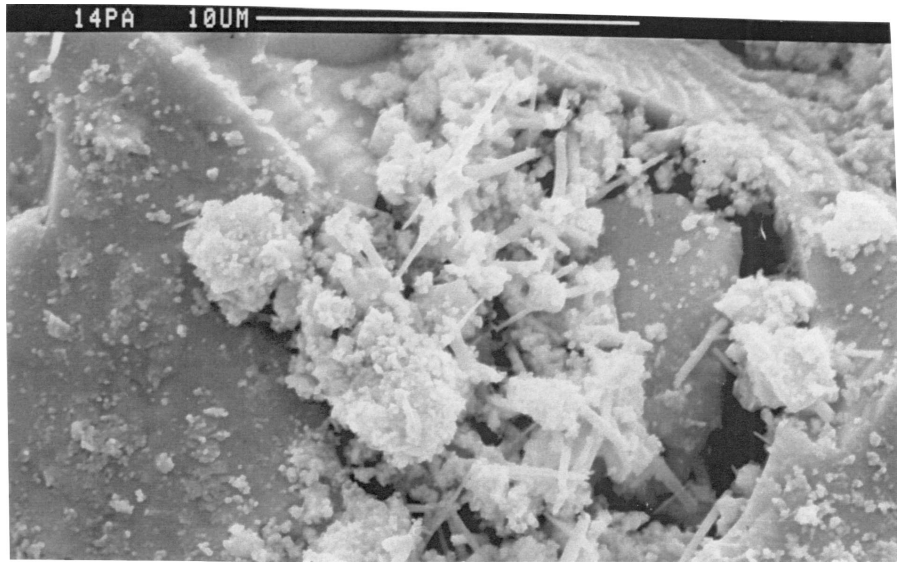

Figure 8 Presence of needle shape compounds in a high humidity condition.

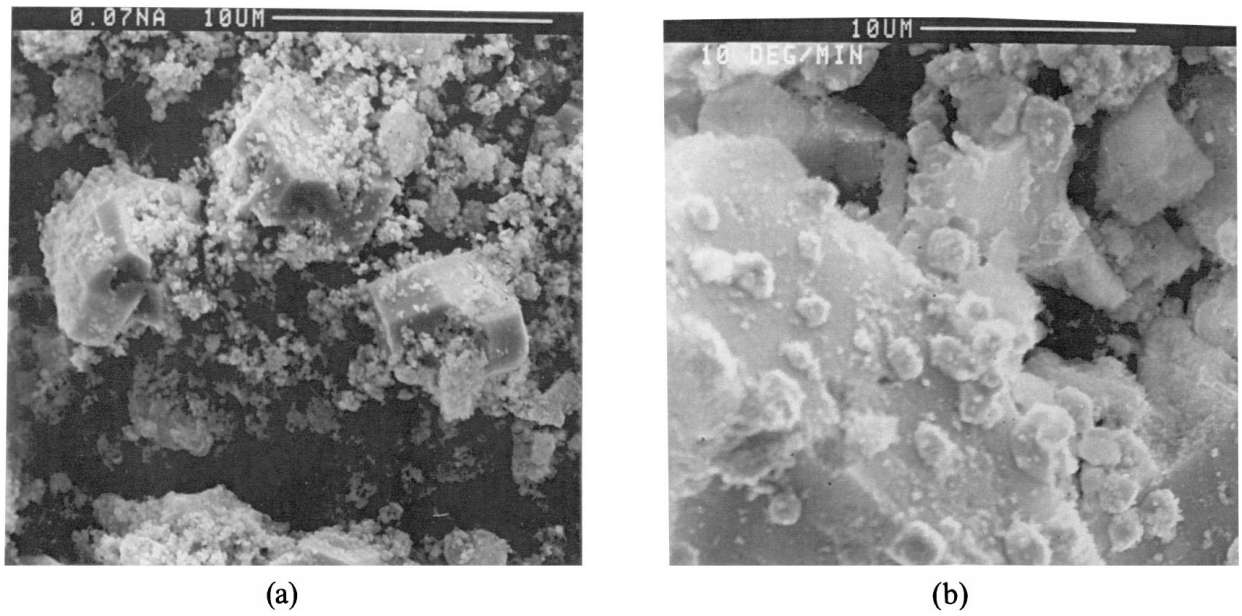

Figure 9 Views of the composite powder for two heating rates. (a) 4 °C/min, (b) 10 °C/min.

Figure 10 Presence of a large tungsten trichite for a high humidity condition.

time of five hours was necessary in order to transform zirconia in the cubic phase without residual monoclinic phase (Table IV).

A relatively slow heating rate (4 °C/min) leads to large tungsten crystals whereas a faster heating rate (10 °C/min) leads to smaller crystals. The composite powder morphology for these two heating rate conditions is shown in Fig. 9. As it has been noted before, the reduction reaction is influenced by the atmosphere humidity, we thus observed that for high humidity condition large tungsten trichites appeared in the powder (Fig. 10). It can be also noted that with the synthesis conditions used in this work there is no reactivity between zirconia and tungsten oxide. Indeed the compound $Zr_2W_2O_8$ which has been evidenced in the ZrO_2–WO_3 phase diagram [28] has never been detected with the mixed precipitates described here.

4. Conclusion

Stabilized zirconia-tungsten composite powders were prepared from metal salts solution using a sol-gel/co-precipitation route without mixing and milling steps. The stability of the mixed suspension as well as the surface area of the dried precipitate and the metal content in the resulting powder can be controlled by the tungsten salts content. The adsorption of the negatively charged tungsten species on the zirconia surface leads to a great repulsive effect between particles. Before the reduction the powder could be described as a supported oxide powder and thus could be tested as catalytic powder. There is a strong interaction between the tungsten species and the zirconia grains. The transformation from the amorphous powder to the composite zirconia-tungsten powder under thermal treatment was described using four temperature ranges. Various tungsten oxide such as WO_3, $WO_{2.9}$, $WO_{2.72}$, and WO_2 were detected during the reduction treatment. The adsorbed tungsten species leads to a shield effect, hence the zirconia formation occurs at higher temperature than for the zirconia single phase case. The morphology of the composite powder is influenced by the humidity and thermal treatment conditions.

References

1. P. COLOMBAN, *l'industrie Céramique* **792** (1985) 186.
2. V. S. STUBICAN, *J. Amer. Ceram. Soc.* **5**(1/2) (1978) 17.
3. K. HABERKO, *Ceram. Int.* **5**(4) (1979) 148.
4. S. RAMANATHAN, *J. Mater. Sci. Lett.* **12** (1993) 122.
5. J. G. DUH and M. Y. LEE, *J. Mater. Sci.* **24** (1989) 4467.
6. R. A. ROY and R. ROY, *Mater. Res. Bull.* **19** (1984) 169.
7. N. Q. MINH, *J. Amer. Ceram. Soc.* **76**(3) (1993) 563.
8. W. H. TUAN and R. J. BROOKS, *J. Europ. Ceram. Soc.* **6** (1990) 31.
9. N. NAWA, K. YAMAZAKI, T. SEKINO and K. NIHARA, *J. Mater. Sci.* **31**(11) (1996) 2849.
10. T. LOPEZ, P. BOSCH and R. GOMEZ, *Reac. Kine. Cat. Let.* **41**(1) (1990) 217.
11. E. BREVAL, *J. Mater. Sci.* **27** (1992) 1464.
12. L. GANAPATHI, G. N. SUBBANA, K. S. NAJUNDASWANY and C. N. R. RAO, *J. Sol. Stat. Chem.* **66** (1987) 376.
13. G. N. SUBBANA and C. N. R. RAO, *Mat. Res. Bull.* **21** (1986) 376.
14. C. J. BRINKER and G. W. SCHERER, "Sol-Gel Science" (Academic Press, 1990).
15. A. CLEARFIELD, *Rev. Pur. App. Chem.* **14** (1964) 91.
16. M. F. DANIEL, B. DESBAT, J. C. LASSEGUE, B. GERAND and M. FIGLARTZ, *J. Sol. Stat. Chem.* **67** (1987) 235.
17. G. RAMIS, C. CRISTIANI, A. S. ELMI, P. VILLA and G. BUSCA, *J. Mol. Cat.* **61** (1990) 319.
18. V. S. NAGARAJAN and K. J. RAO, *J. Mater. Sci.* **24** (1989) 2140.
19. A. IANNIBELLO, P. L. VILLA and S. MARENGO, *Gaz. Chim. Ital.* **109** (1979) 521.
20. F. HANIC, M. HARTMANOVA, A. A. URUSOVSKAYA, G. G. KNAB, N. A. IOFIS and I. L. ZYRYANOVA, *Sol. Stat. Ion.* **36** (1989) 197.
21. M. HINO and K. ARATA, *J. Chem. Soc. Chem. Com.* **18** (1988) 1259.
22. J. L. WALTER and K. L. LOU, *J. Mater. Sci.* **24** (1989) 3577.
23. W. D. SCHUBERT, *Int. J. Refr. Hard. Met.* **9**(4) (1990) 178.
24. R. C. GAVIE, *J. Phy. Chem.* **69**(4) (1965) 1238.
25. P. TITTARELLI, A. IANNIBELLO and P. L. VILLA, *J. Sol. Stat. Chem.* **37** (1981) 95.
26. C. CHOAIN and F. MARION, *Compt. Ren. Acad. Sci.* **258** (1961) 3258.
27. J. BOUSQUET and G. PERACHON, *ibid.* **258** (1964) 3869.
28. L. L. Y. CHANG, M. G. SCROGER and B. PHILIPS, *J. Amer. Ceram. Soc.* **50**(4) (1967) 212.

Received 29 July 1998
and accepted 27 January 1999